International
Progress Report

IPR-03-43

Äspö Hard Rock Laboratory

TRUE Block Scale continuation project

Significance of diffusion limitations and rim zone heterogeneity for tracer transport through fractures at the Äspö site

Vladimir Cvetkovic

Water Resources Engineering KTH

November 2003

Svensk Kärnbränslehantering AB
Swedish Nuclear Fuel
and Waste Management Co
Box 5864
SE-102 40 Stockholm Sweden
Tel +46 8 459 84 00
Fax +46 8 661 57 19

Äspö Hard Rock
Laboratory

Report no.
IPR-03-43
No.
F56K
Author
Vladimir Cvetkovic
Date
Nov. 2003
Checked by
Anders Winberg
Date
Nov. 2003
Approved
Christer Svemar
Date
2004-01-22

Äspö Hard Rock Laboratory

TRUE Block Scale continuation project

Significance of diffusion limitations and rim zone heterogeneity for tracer transport through fractures at the Äspö site

Vladimir Cvetkovic

Water Resources Engineering KTH

November 2003

Keywords: Tracer transport, crystalline rock, retention in fractures, transport modelling, rim zone, limited diffusion, retention heterogeneity

Contents

1 Introduction **11**

1.1 TRUE findings 11

1.2 Problem formulation and objectives 12

2 Transport model **13**

2.1 Lagrangian formulation 13

2.1.1 Unlimited diffusion 14

2.1.2 Limited diffusion 15

2.2 Transport predictions 15

2.2.1 Unlimited diffusion 15

2.2.2 Limited diffusion 16

3 Assumptions for sensitivity analysis **19**

3.1 Retention zone heterogeneity 19

3.2 Injection conditions 25

3.3 Advective travel times 25

3.4 Tracer selection 26

4 Computations **27**

5 Results **29**

5.1 Tritium 29

5.2 Barium 32

5.3 Cesium 37

6 Summary and conclusions **43**

Abstract

We study the potential impact of a limited rim zone and its spatially variable porosity, on tracer breakthrough under conditions comparable to those of TRUE-1 and TRUE Block Scale. For this task, we adopt a relatively simple, semi-analytical Lagrangian approach (Cvetkovic et al., 2000; Cvetkovic and Cheng, 2002). A rim zone is assumed to exist with a spatially variable extent (thickness) and variable porosity in the direction of the fracture plane; retention is assumed to take place in the rim zone only. Retention properties are assumed consistent with those estimated for Feature A in TRUE-1 tests; the extent of the rim zone and its correlation to porosity, are treated as sensitivity parameters. We find that finite injection (or tailing in the injection) will generally "mask" the impact of diffusion limitations, by making it much less apparent (or apparent much later). A rim zone up to 10 mm thick (4.1 mm in the mean) appears sufficient for observations of diffusion limitations to be virtually impossible for Cs, relatively difficult for Ba, and possible for HTO, even if there is tailing in the injection and the mean water residence time is in the range 10-100 h. The presented methodology can be further used for estimating potential effects in the forthcoming tests within TRUE BS2A, for re-evaluating breakthrough curves of already completed tests (TRUE-1 and TRUE Block Scale), as well as for assessing the possible impact of diffusion limitations for long-term radionuclide transport.

Sammanfattning

Vi studerar hur diffusion/sorption i en begränsad retentionszon (s k ”rim zone”), zonens tjocklek och den rumsliga variabilitet i porositet kan påverka transporten av spårämnen i bergssprickor i Äspöområdet; transportförhållandena för analysen stämmer överens med förhållandena i TRUE-1- och TRUE-Block-Scale-testerna. Ett relativt enkelt, semi-analytiskt modelleringskoncept används för analysen. Vi antar att sprickorna har en begränsad retentionszon med varierande tjocklek och att retentionen sker enbart i den zonen. Vi finner att spårämnesinjektion med lång svans kan dölja effekten av en begränsad retentionszon, så att den är i praktiken svår att observera i genombrottskurvor. Påverkan av en retentionszon som är upp till 10 mm tjock (4.1 mm i medelvärde) kan vara möjlig att observera för HTO, svår att observera för Ba och i praktiken omöjlig att observera för Cs, om injektionskurvan har svans och medelankomsttiden för vatten är mellan 10-100 h. Den analysmetod vi presenterar kan användas på olika sätt: för att prediktera vilka effekter en begränsad retentionszon skulle kunna ha på kommande tester inom TRUE BS2A; för att omvärdera befintliga data från tidigare spårämnesförsök och möjligtvis uppskatta tjockleken på retentionszonen; samt för att studera vilka effekter en begränsad retentionszon skulle kunna ha på långtidstransporten av radionuklider i Äspöområdet.

Executive summary

Laboratory investigations of intercepts from the TRUE-1 site yield a porosity in the vicinity of fractures (rim zone, including breccia) in the range from one to a few percent; this can be compared to the porosity of the unaltered rock that is typically in the range 0.1-0.5%. Laboratory investigations also indicate that porosity adjacent to a fracture varies spatially. We adopt here a relatively simple, semi-analytical approach of following trajectories along a flow path (Cvetkovic and Cheng, 2002) to study the potential impact of a limited rim zone and its spatially variable porosity, on the outcome of tracer tests, in particular under conditions comparable to those of the TRUE-1 and TRUE Block Scale tests.

We consider a flow (or transport) path through one or several fractures, where retention properties can vary along the flow path. We assume the existence of a *rim zone* defined as a zone adjacent to the fracture with distinct retention properties relative to the unaltered rock. Retention is assumed to take place in the rim zone only, putting emphasis on the role of the rim zone for transport. The assumed retention properties of the rim zone are consistent with those estimated for Feature A in TRUE-1 tests, while its extent is treated as a sensitivity parameter.

We find that finite injection (or tailing in the injection) will generally "mask" the impact of diffusion limitations, by making it much less apparent (or apparent much later), in particular for non-sorbing and weakly sorbing tracers. For HTO, for instance, effect of diffusion limitations would be observable after 50 h if an ideal pulse was injected, and after almost one year if finite injection is applied. A rim zone up to 10 mm thick (4.1 mm in the mean) appears sufficient for observations of diffusion limitations to be virtually impossible for Cs, relatively difficult for Ba, and possible for HTO, even if there is tailing in the injection (as in TRUE-1) and the mean water residence time is in the range 10-100 h. Spatial variability in the rim zone thickness and porosity (diffusivity) has comparatively little impact on the BTCs, relative to the case where effective parameters are used (here defined as arithmetic mean).

The presented methodology can be applied in order to assess the possible impact of diffusion limitations on the results of the forthcoming tests within TRUE BS2A. The presented methodology could also be used to re-evaluate the breakthrough curves of already completed tests (TRUE-1 and TRUE Block Scale), in order to assess possible evidence of diffusion limitations and estimate an average extent of the rim zone. Finally, the methodology could be applied for assessing the possible impact of diffusion limitations for long-term radionuclide transport.

Chapter 1

Introduction

The TRUE programme addresses radionuclide retention in crystalline rock from the laboratory scale, to the scale of approximately 30-50 m. The main purpose of the TRUE tests is to improve the understanding of retention mechanisms and hence increase the confidence in modelling retention on spatial and temporal scales relevant for PA/SA. The central issue addressed in the TRUE programme is one of *scale transition*, or extrapolation, from the laboratory, to the near-field (TRUE) scale, as a basis for further extrapolation to the far-field scale.

1.1 TRUE findings

One of the main finding of the TRUE tests carried so far, has been relatively strong retention, compared to what was expected based on laboratory investigations on core samples of unaltered rock. These findings were interpreted as a result on the one side of enhanced retention properties of the rock adjacent to the fractures along the flow paths, and on the other due to the presence of small rock fragments (breccia) and gouge material in the fractures.

Laboratory data on retention properties using intercept samples, provided values of porosity, and of microscopic structure and composition (mineralogy) of the rock adjacent to the fractures (Byegård et al., 2001; Kelokaski et al., 2001). This data indicates two specific features:

- a relatively thin layer of enhanced porosity where most of the retention presumably takes place (referred to as the *rim zone*);
- random spatial variability of both the porosity of the rim zone, and of the extent of the rim zone.

The porosity of the unaltered rock was found to be in the range 0.1-0.5%, whereas in the vicinity of fractures (rim zone, including breccia) the porosity was found to be in the range from one to a few percent. Thus strictly we have three-dimensional variability, with a clear trend of decreasing porosity from the altered rock adjacent to the fracture, toward the intact rock of the unaltered matrix. A full three-dimensional deterministic transport

model can in principle be used for Monte Carlo simulations in order to capture the random variability. An alternative, simpler approach used for interpreting TRUE-1 and TRUE Block Scale results (Cvetkovic et al., 1999; Cvetkovic et al., 2000; Cvetkovic and Cheng, 2002), follows trajectories along a flow path and can account for the limited extent of the rim zone and its spatially variable porosity. The latter approach is to be adopted in this study.

1.2 Problem formulation and objectives

We consider a flow (or transport) path through one or several fractures, from an injection to a detection point (borehole). The flow path is conceptualized as consisting of many trajectories (streamlines, or streamtubes). Flow velocity generally varies along trajectories, whereby the advective travel time associated with a trajectory, τ, is a random variable. Retention properties of the rim zone can also vary along the trajectories of the flow path.

We assume the existence of a *rim zone* defined as a zone adjacent to the fracture with distinct retention properties (in this study porosity and diffusivity), relative to the unaltered rock. Retention is assumed to take place in the rim zone only, i.e., we simplify the problem by neglecting the retention that would take place in the unaltered rock once the rim zone is saturated. This simplification puts more emphasis on the role of the rim zone for transport, and will affect the transport only at later times.

The assumed retention properties of the rim zone are consistent with those estimated for Feature A in TRUE-1 tests, while its extent (denoted as ζ [L]) is treated as a sensitivity parameter. The parameter ζ is treated as uniform or spatially variable along a trajectory, following a model that will be specified in section 4.1. The porosity of the rim zone θ is also treated as uniform or spatially variable along the flow path; two limiting cases of correlation between θ and ζ will be considered: Perfect positive and negative correlation.

Objectives of this report are:

- To present a semi-analytical (Lagrangian) model for tracer transport between an injection and detection borehole where diffusion is limited to the rim zone and retention properties are spatially variable.
- To study the potential impact of diffusion limitations, assuming material properties, flow and injection conditions corresponding to those for TRUE-1 and TRUE Block Scale tracer tests.

Chapter 2

Transport model

Advection and dispersion through fractures coupled with retention in the rim zone are to be modelled using the dual-porosity concept (Neretnieks, 1980; Cvetkovic et al., 1999).

2.1 Lagrangian formulation

Let a tracer particle be injected at point A and detected at point B; transport of the particle takes place along a trajectory through one or several interconnected fractures. The probability density function of the particle residence time is written in a general form in the Laplace domain as (Cvetkovic et al., 1998)

$$\widehat{\gamma} = \exp\left\{-s\tau - s\int_0^\tau \widehat{g}[s, \mathbf{X}(\varphi)]\, d\varphi\right\} \tag{2.1}$$

where $\widehat{()}$ denotes Laplace transform, s is the Laplace transform variable, $g(t, \mathbf{x})$ is the memory function which contains information on spatially variable retention processes, and $\mathbf{X}(t)$ is the usual Lagrangian formulation of a trajectory (e.g., Dagan, 1984).

It is convenient for applications to adopt a discretized version of Eq.(2.1) whereby a trajectory is viewed as a one-dimensional lattice, and the transport as a "walk" between adjacent lattice sites (Cvetkovic and Haggerty, 2002). We re-write Eq.(2.1) as

$$\widehat{\gamma} = \exp\left[-s\tau - s\sum_i \widehat{g}_i(s)\,\tau_i\right] \tag{2.2}$$

where the lattice sites $i = 1, N$ can be interpreted either within a single fracture, or between fractures if a fracture network with many connected fractures is considered[1]. Increment of the water residence time at a given site (location) i is τ_i, and we have

$$\tau = \sum_i \tau_i$$

Two distinct models of retention are to be compared in this report.

[1] In the intermediate case, say of a few interconnected fractures, it is appropriate to introduce double indices say i and j where i would denote a site within fracture j (Cvetkovic and Cheng, 2002); here for simplicity we use only one index.

2.1.1 Unlimited diffusion

This is the classical case extending the model originally proposed by Neretnieks (1980), where one-dimensional, Fickian diffusion with sorption takes place in an infinite rock matrix. In this case, the Laplace transform of the discrete memory function g_i in Eq.(2.2) is defined by

$$\widehat{g}_i(s) = \frac{\kappa_i}{b_i}\,\frac{1}{\sqrt{s}} \quad ; \qquad \kappa_i \equiv \theta_i\,\sqrt{D_i R_i} \tag{2.3}$$

where θ is matrix porosity, D is pore diffusivity, and R is the retardation coefficient $R = 1+(1-\theta)\rho K_d/\theta$, with ρ [M/L^3] being the rock matrix density and K_d [L^3/M] the sorption coefficient; in general all parameters are variable along a trajectory (streamline), hence index i.

Laplace inversion of Eq.(2.3) yields

$$g_i(t) = \frac{\kappa_i}{b_i}\,t^{-1/2} \tag{2.4}$$

whereby Eq.(2.1) can also be inverted to yield

$$\gamma(t) = \frac{H(t-\tau)\,B}{2\sqrt{\pi}(t-\tau)^{3/2}}\,\exp\left[\frac{-B^2}{4(t-\tau)}\right] \tag{2.5}$$

where

$$B \equiv \sum_i \frac{\kappa_i\,\tau_i}{b_i} \tag{2.6}$$

and $H(\cdot)$ is the Heaviside step function. It can be shown that the peak of γ is proportional to $1/B^2$ and the peak arrival time is proportional to B^2; B^2 [T] may in fact be referred to as the "retention time", providing a simple and useful direct measure of retention (Cvetkovic et al., 2003).

If retention parameters θ, K_d and D are all *uniform* along a trajectory, then

$$B = \kappa\beta \quad ; \quad \beta = \sum_i \frac{\tau_i}{b_i} \qquad \kappa = \theta\sqrt{D\,R} \tag{2.7}$$

For a structurally uniform fracture where the aperture is constant, the flow path is a rectangular "channel" of width W [L] and length L [L], carrying a volumetric flow rate q [L^3/T]. In this case,

$$B = \kappa\beta \quad ; \quad \beta = \frac{2LW}{q}$$

and we recover from Eq.(2.5) the basic result of Neretnieks (1980).

A common assumption in the evaluation of TRUE tracer tests, as well as in PA/SA, is that β can be linearized in τ, as

$$\beta = k\,\tau \quad ; \quad k \equiv \frac{1}{b_{\rm ret}} \tag{2.8}$$

where $2b_{\rm ret}$ is an effective "retention" aperture, for a given fracture or a network of fractures. This assumption replaces a heterogenous fracture (or network of fractures) with a homogeneous "effective" fracture and the key problem is determining $2b_{\rm ret}$, for instance, from the correlation slope between τ and β if simulations are used (Cvetkovic et al., 2000; Cvetkovic et al., 2003).

2.1.2 Limited diffusion

Let the retention zone of a given segment i be of limited extent, denoted by ζ_i; we can refer to this finite zone also as the "rim" zone. Then the Laplace transform of the memory function g_i in Eq.(2.2) is defined as (Cvetkovic et al., 1999)

$$\widehat{g}_i(s) = \frac{\kappa_i}{b_i} \frac{A_i(s)}{\sqrt{s}} \tag{2.9}$$

where

$$A_i(s) \equiv \frac{\exp\left\{2\,\zeta_i\,[s\,R_i/D_i]^{1/2}\right\} - 1}{\exp\left\{2\,\zeta_i\,[s\,R_i/D_i]^{1/2}\right\} + 1} \tag{2.10}$$

For $\zeta \to \infty$, $A \to 1$ and we recover the unlimited diffusion case Eq.(2.3).

2.2 Transport predictions

Let the total injected tracer mass be m [M] and the injection rate ϕ [1/T]. Then tracer discharge at the detection point B (denoted as J [M/T]) is given by:

$$J(t) = m\ \langle \phi * \gamma \rangle \tag{2.11}$$

where "*" denotes convolution, and the averaging is over all streamlines (trajectories) which constitute a flow path between the pumping and detection locations, A and B. With ϕ specified and identical for all streamlines, we have

$$J(t) = m\,[\phi(t)\ *\ h(t)] \tag{2.12}$$

where $h(t) \equiv \langle \gamma \rangle$ is an unconditional probability density function (pdf) of particle residence time from point A to B. If the volumetric flow rate which discharges the tracer at point B is q [L^3/T], then the measurable tracer concentration C [M/L^3] at B is evaluated as

$$C(t) = \frac{J(t)}{q} \equiv \frac{m}{q} \int_0^t \phi(t-t')\,\langle \gamma(t') \rangle\, dt'. \tag{2.13}$$

We discuss below different ways of computing h, depending on the type of retention heterogeneity.

2.2.1 Unlimited diffusion

If the retention zone is unlimited and Eq.(2.3) is applicable, then we compute h as

$$h(t) \equiv \langle \gamma \rangle = \int \gamma(t|\tau, B)\ f(\tau, B)\, d\tau\, dB \tag{2.14}$$

where f is a joint pdf for τ and B. If the retention parameters are uniform then Eq.(2.8) is applicable and we have

$$h(t) \equiv \langle \gamma \rangle = \int \gamma(t|\tau, \beta)\ f(\tau, \beta)\, d\tau\, d\beta \tag{2.15}$$

We note that the joint pdf $f(\tau, \beta)$ is dependent only on advective/structural properties of the fractures, and not on retention properties.

2.2.2 Limited diffusion

If the rim zone is of limited extent with Eq.(2.9) applicable in the general case, then a closed form γ is not available and consequently h cannot be written in an integral form as Eq.(2.14) or Eq.(2.15). In this case, a Monte Carlo computational approach can be used, whereby the ensemble average is performed over many realizations of the trajectories. We explore different means for simplifying the calculations.

If the discretization segments (or lattice sites) are viewed in the temporal domain, then the tracer particle takes steps along a time axis τ, rather than the conventional spatial domain (Cvetkovic and Haggerty, 2002). In such a case, the integral (summation) term in Eq.(2.1)-Eq.(2.2) can be written as

$$\int_0^\tau g(s,\vartheta)d\vartheta = \sum_i \widehat{g}_i(s)\,\tau_i = \Delta\tau \sum_{i=1}^{N} \frac{1}{b_i}\frac{A_i(s)}{\sqrt{s}}\,\kappa_i \tag{2.16}$$

where the time increment $\Delta\tau$ is specified as a constant. We consider N equal steps, or segments, where retention parameters are assigned values for each step $i = 1, N$, and write

$$\sum_i \widehat{g}_i(s)\,\tau_i = N\,\Delta\tau\,\frac{1}{\sqrt{s}}\left[\frac{1}{N}\sum_{i=1}^{N}\frac{\kappa_i}{b_i}\,A_i(s)\right] = \tau\,\frac{1}{\sqrt{s}}\left[\frac{1}{N}\sum_{i=1}^{N}\frac{\kappa_i}{b_i}\,A_i(s)\right] \tag{2.17}$$

since by definition $\tau = N\Delta\tau = \sum \tau_i$.

If the trajectories are sufficiently long relative to the integral scale of the variable parameters such that the ergodic hypothesis is applicable, we may replace the average in the brackets on the RHS of Eq.(2.17) by an ensemble average as

$$\sum_i \widehat{g}_i(s)\,\tau_i \approx \tau\,\frac{1}{\sqrt{s}}\left\langle\frac{\kappa}{b}\,A(s)\right\rangle \tag{2.18}$$

where angular brackets denote ensemble averaging along the flow path. Equation (2.18) defines the summation term of Eq.(2.2) as being proportional to an expected value, with the Laplace transform variable s as a parameter. The computations based on Eq. (2.18) are complicated by the fact that in general, the expected value is not constant with respect to τ.

The parameters that are being averaged in Eq. (2.18) (i.e., the material properties group κ, the rim zone parameters in $A(s)$ and the half-aperture b) are all Lagrangian as they follow trajectories; hence in principle they all depend on the trajectory $\mathbf{X}(t)$ and thereby on advective travel time τ. We shall simplify our following analysis in two ways:

- We neglect the possible correlation between the structural properties as quantified by the aperture $2b$, and the retention properties as quantified by parameters in κ and A. We can then write

$$\left\langle\frac{\kappa}{b}\,A(s)\right\rangle \approx \left\langle\frac{1}{b[\mathbf{X}(\tau)]}\right\rangle\,\langle A(s)\,\kappa\rangle \tag{2.19}$$

- We assume that

$$\left\langle \frac{1}{b[\mathbf{X}(\tau)]} \right\rangle \approx \frac{1}{b_{\rm ret}} \tag{2.20}$$

where $2b_{\rm ret}$ is the "retention aperture" associated with β and defined in Eq. (2.8).

The evolution of distinct properties of the rim zone are related to geochemical processes facilitated by the flow. Moreover, a feedback mechanism may have been present over long times, where the flow affected the properties of the rim zone (porosity and thickness) and then these properties to some extent affected flow. Thus it is conceivable that the porosity and thickness of the rim zone, are to some extent correlated to the fracture aperture locally. At this time, we do not have sufficient information to establish such a correlation. Although such a correlation could be considered as part of the sensitivity, we shall neglect it in the present analysis and limit the sensitivity to the correlation between the rim zone thickness ζ and porosity θ, as quantified by the variability parameter w.

The calculation of h can be simplified by taking advantage of the above assumptions; we now re-write Eq.(2.18) as

$$\sum_i \widehat{g}(s)\tau_i \approx \tau \, \frac{1}{\sqrt{s}} \, \frac{1}{b_{\rm ret}} \, \langle A(s)\, \kappa \rangle \equiv \tau \, k \, \frac{1}{\sqrt{s}} \, \langle A(s)\, \kappa \rangle \tag{2.21}$$

Note that in Eq.(2.21), a structurally heterogeneous fracture is replaced by a homogeneous (effective) one based on Eq. (2.8), but the variability in retention properties is retained.

Inserting Eq.(2.21) into Eq.(2.2) we get

$$\widehat{\gamma} = \exp\left\{ -\tau \, \left[s + k\,\sqrt{s} \, \langle A(s)\, \kappa \rangle \right] \right\} \tag{2.22}$$

where τ is the only random variable since $\langle A(s)\, \kappa \rangle$ has been assumed constant for a given flow path (i.e., for all trajectories) and independent of τ.

To compute h, we take the expected value of γ Eq.(2.22) and obtain in the Laplace domain

$$\widehat{h}(s) = \langle \widehat{\gamma} \rangle = \int \widehat{\gamma}(s|\tau)\, f(\tau)\, d\tau \tag{2.23}$$

where $f(\tau)$ is the water residence time density. Inserting Eq.(2.22) into Eq.(2.23), we have

$$\widehat{h}(s) = \int \, \exp\left\{ -\tau \, \left[s + k\, E(s) \sqrt{s} \right] \right\} \, f(\tau)\, d\tau \tag{2.24}$$

where

$$E(s) \equiv \langle A(s)\, \kappa \rangle$$

If the Laplace transform of $f(\tau)$ is available, then the form Eq.(2.24) enables a relatively simple computation of $\widehat{h}$ as (Cvetkovic et al., 1998)

$$\widehat{h}(s) = \widehat{f}\,[\mathcal{W}(s)] \tag{2.25}$$

where

$$\mathcal{W}(s) \equiv s + k\, E(s)\sqrt{s} \tag{2.26}$$

Analytical or numerical inversion of $\widehat{f}\,[\mathcal{W}(s)]$ yields the desired solution for h. Finally, we compute the normalized tracer discharge J/m in the Laplace domain as

$$\frac{\widehat{J}(t)}{m} = \widehat{\phi}\,\widehat{h} = \widehat{\phi}(s)\;\widehat{f}[\mathcal{W}(s)] \tag{2.27}$$

where $E(s)$ is written in full as

$$E(s) \equiv \langle A(s)\,\kappa\rangle = \left\langle \theta\,\sqrt{DR}\;\frac{\exp\left\{2\,\zeta\,[s\,R/D]^{1/2}\right\} - 1}{\exp\left\{2\,\zeta\,[s\,R/D]^{1/2}\right\} + 1}\right\rangle \tag{2.28}$$

In general, all the parameters θ, R, D and ζ are variable along trajectories. For specified distributions of θ, R, D and ζ, we can compute E for a given s, and therefrom compute h and J by Laplace inversion. The measurable tracer concentration at the pumping location B is then $C(t) = J(t)/q$, Eq.(2.13).

If the rim zone is sufficiently large (formally $\zeta \to \infty$), we have $A(s) \to 1$ and $E = \langle\kappa\rangle$, whereby Eq.(2.24) reduces to the unlimited diffusion case with variable retention parameters which has been considered earlier (Cvetkovic et al., 2000).

Chapter 3

Assumptions for sensitivity analysis

We shall consider here the following variants in the sensitivity analysis:

1. A non-sorbing tracer (HTO), moderately sorbing tracer (Ba) and strongly sorbing tracer (Cs), consistent with the tracers used in the TRUE experiments; the interest is to see how diffusion limitations affect transport depending on the sorption properties of a tracer.

2. Three statistical models of ζ, θ variability are to be used in the analysis: One where the rim zone is relatively thick (ζ is large) with a low porosity θ (negative correlation), one where the rim zone is relatively thin (ζ is small) with high porosity θ (negative correlation), and one where the rim zone is relatively thin with low porosity (positive correlation).

3. Two types of boundary conditions for transport (injection modes): Pure pulse and pulse with a tailing, where the latter is designed to mimic injection conditions of the TRUE tests; the interest is to see if/how the impact of diffusion limitations is influenced by the injection conditions.

4. Two values of the mean water residence times: 10 h and 100 h, designed to cover the range of the TRUE tracer tests; the interest is to see if and how water residence time affects the impact of diffusion limitations.

3.1 Retention zone heterogeneity

First, we shall deterministically relate matrix diffusivity and porosity using Archie's law in order to reduce the number of parameters. Pore diffusivity and porosity are related as $D\theta = D_w F$ where D_w is the diffusivity in water, and F is the formation factor, whereby $D = D_w F/\theta$. Archie's law implies $F = \theta^m$ where m is a parameter here to be assumed as 1.5 (Cvetkovic et al., 2000); then $D = D_w\sqrt{\theta}$. Inserting $D = D_w\sqrt{\theta}$ in Eq.(2.28), we

have

$$E(s) = \left\langle \sqrt{\theta^{2.5}\, D_w\, R}\; \frac{\exp\left[2\,\zeta\sqrt{s\,R/D_w\sqrt{\theta}}\right] - 1}{\exp\left[2\,\zeta\sqrt{s\,R/D_w\sqrt{\theta}}\right] + 1} \right\rangle \tag{3.1}$$

which has reduced the variable parameters of E to three: θ, R and ζ.

The retardation coefficient of the rock matrix is defined by $R = 1 + \rho K_d/\theta$ where ρ is the rock density and K_d is the sorption coefficient. Our further simplification is that the sorption coefficient K_d, as well as the rock density ρ, are uniform. Although K_d presumably also varies, we currently do not have sufficient information and choose to simplify the calculations for illustration purposes.

The number of variable parameters is now reduced to two: finite thickness of the rim zone ζ, and matrix porosity θ. For our sensitivity analysis, we shall consider positive and negative correlation between ζ and θ. Note that R is variable due to variability in θ.

The parameter group E Eq.(3.1) can be written as

$$E(s) = \langle \mathcal{F}(\zeta, \theta \mid s) \rangle \tag{3.2}$$

where

$$\mathcal{F} \equiv \sqrt{\theta^{2.5}\, D_w\, R}\; \frac{\exp\left[2\,\zeta\sqrt{s\,R/D_w\sqrt{\theta}}\right] - 1}{\exp\left[2\,\zeta\sqrt{s\,R/D_w\sqrt{\theta}}\right] + 1}$$

and we emphasize the parametrization with respect to the Laplace transform variable s. The assumption of perfect correlation between θ and ζ implies that their randomness is derived from a single random variable, Z. Then

$$E(s) = \langle \mathcal{F}[\zeta(Z), \theta(Z) \mid s] \rangle = \int \mathcal{F}[\zeta(Z), \theta(Z) \mid s]\, p(Z)\, dZ = \int_0^1 \mathcal{F}[\zeta(P), \theta(P) \mid s]\, dP \tag{3.3}$$

where $p(Z)$ is a specified pdf of Z, and P is the cumulative distribution function (CDF). The usual relationship $p(Z) = dP/dZ$ or $dP = p\, dZ$, holds, where p is the pdf. The functions $\theta(P)$ and $\zeta(P)$ thus specify the statistical model.

A discretized form of Eq.(3.3) is

$$E(s) = \Delta P \sum_i^N \mathcal{F}[\zeta(P_i), \theta(P_i) \mid s] \tag{3.4}$$

For illustration purposes, we consider the following functional form

$$Y(P) = Y_0 + \frac{1}{w}\,(Y_2 - Y_1)\,\ln[1 - (1 - \mathrm{e}^w)\,P] \tag{3.5}$$

where Y stands for either ζ or θ,

$$a \equiv \frac{w}{Y_2 - Y_1} \quad ; \quad Y_1 \le Y \le Y_2 \quad ; \quad w \neq 0 \tag{3.6}$$

and Y_1 and Y_2 denote lower and upper bounds of Y, respectively.

Equation Eq.(3.5) corresponds to a bounded exponential model for θ and ζ, in the form

$$P(y) \equiv \text{Prob}\{y \leq Y\} = \frac{1 - \mathrm{e}^{a\,(Y - Y_1)}}{1 - \mathrm{e}^{w}} \tag{3.7}$$

The pdf of Y, $p(Y)$, is obtained by differentiation of $P(Y)$ as

$$p(Y) = \frac{a}{\mathrm{e}^{w} - 1}\, \mathrm{e}^{a(Y - Y_1)} \tag{3.8}$$

For $w \to \infty$, $p(Y)$ converges to a uniform distribution in the interval Y_1, Y_2, i.e., $p(Y) \to 1/(Y_2 - Y_1)$. For $w \to 0$, $p(Y)$ converges to a Dirac delta distribution; specifically for $w \to +0$, $p(Y) \to \delta(Y - Y_2)$, and for $w \to -0$, $p(Y) \to \delta(Y - Y_1)$.

The mean value $\langle Y \rangle$ is obtained by integration as

$$\langle Y \rangle = \int Y\, p(Y)\, dY = \frac{1}{\mathrm{e}^{w} - 1} \left[\frac{1}{a}\, (1 - \mathrm{e}^{w}) + \mathrm{e}^{w}\, Y_2 - Y_1 \right] \tag{3.9}$$

The porosity θ and the retention zone thickness ζ are defined between two limiting values, denoted as θ_1, θ_2 (minimum, maximum) and ζ_1, ζ_2 (minimum, maximum), respectively. The minimum values are to be fixed as $\theta_0 = 0.004$ and $\zeta = 1$ mm, and the maximum values as $\theta_2 = 0.04$ and $\zeta_2 = 10$ mm. These limits are not based directly on measurements, but are derived indirectly from measurements; with these limits (and a specific value of w), the variability model Eq. (3.8) yields a consistent comparison with one set of available data, as will be shown below.

The parameter w will be assigned different values in the sensitivity analysis. The sign of w decides the shape of the distribution: For $w < 0$ the distribution is skewed to the left, and for $w > 0$ it is skewed to the right. If w for θ and ζ has opposite signs, then we have perfect negative correlation. The magnitude of w governs the mean value (and/or the form of the distribution) and is a key sensitivity parameter.

We show in Figure 3.1 the CDFs for the three statistical models (denoted as Models 1,2 and 3) that will be used for illustration. As can be seen from the form of the CDFs, as well as from the mean values, Model 1 implies a relatively thick retention zone (mean 7.9 mm) and a relatively small mean porosity of 1.2%, thus the two are negatively correlated. Model 2 also implies negative correlation, however, in this case we have a relatively thin retention zone (mean 3.1 mm) and a relatively large mean porosity of 3.2%. Finally, Model 3 assumes positive correlation where the mean values are consistent with (limited) data available from the TRUE-1 Feature A intercepts (Byegård et al., 2001). The comparison of the mean ζ with the profile porosity measurements is shown in Figure 3.3, as well as the pdf of Model 3 compared for θ with two data sets. The mean values are given in Figure 3.2 as functions of w. We see convergence to a uniform distribution for $w \to 0$, and to step distributions (deterministic values) for $w \to \infty$.

The expressions $\zeta(P)$ and $\theta(P)$ are intuitive since they reflect the spatial aspect of the variability in ζ and θ. The probability P can be viewed as the normalized distance along a trajectory in view of the ergodicity assumption; for instance, $P = 0.4$ in Figure 3.1 for Model 1 would imply that 40% of the trajectory length has a porosity below 0.8%, and retention zone depth below 8 mm.

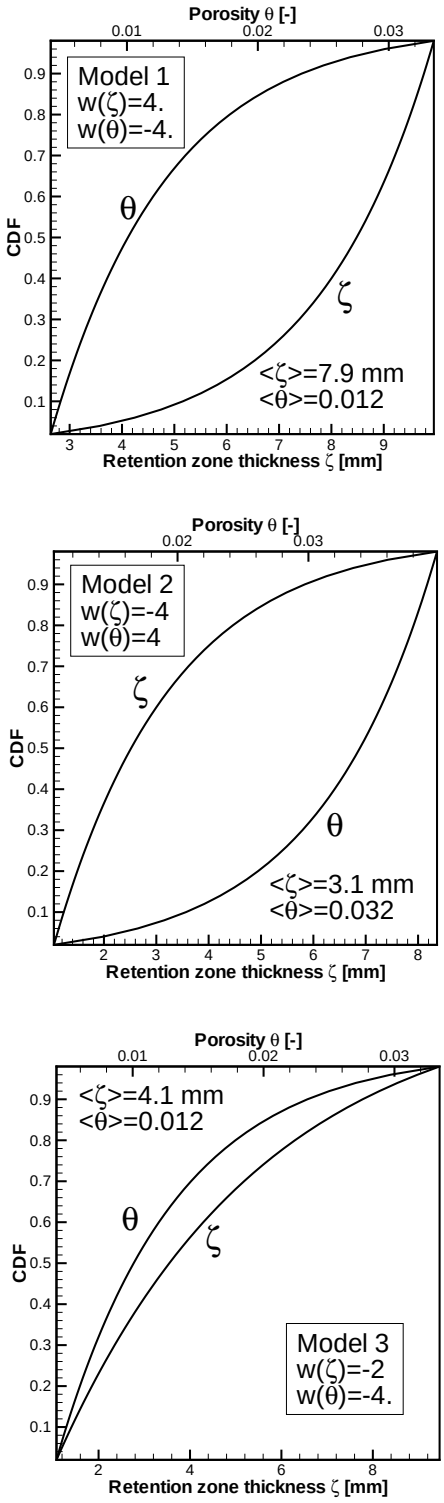

Figure 3.1: *Functional dependence $\zeta(P)$ and $\theta(P)$ based on Eq.*(3.5) *for three different variability models used in the sensitivity analysis: Model 1, Model 2 and Model 3; the parameters $w(\zeta)$ and $w(\theta)$ are specified in the figures.*

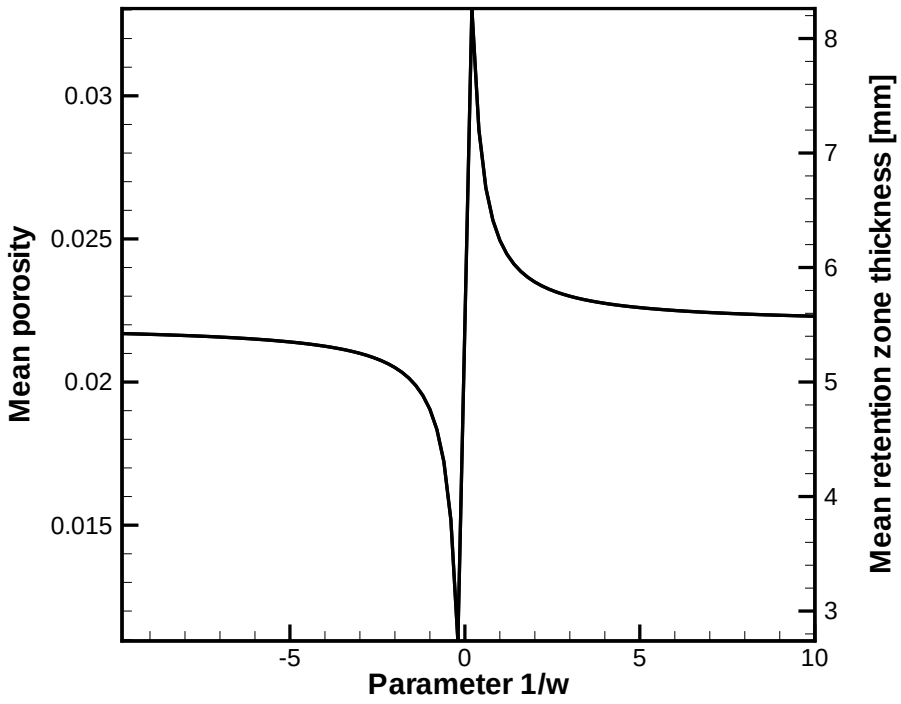

Figure 3.2: *Dependence of the mean ζ and θ as defined in Eq.*(3.9) *on the parameter w (here conveniently given as dependence on $1/w$).*

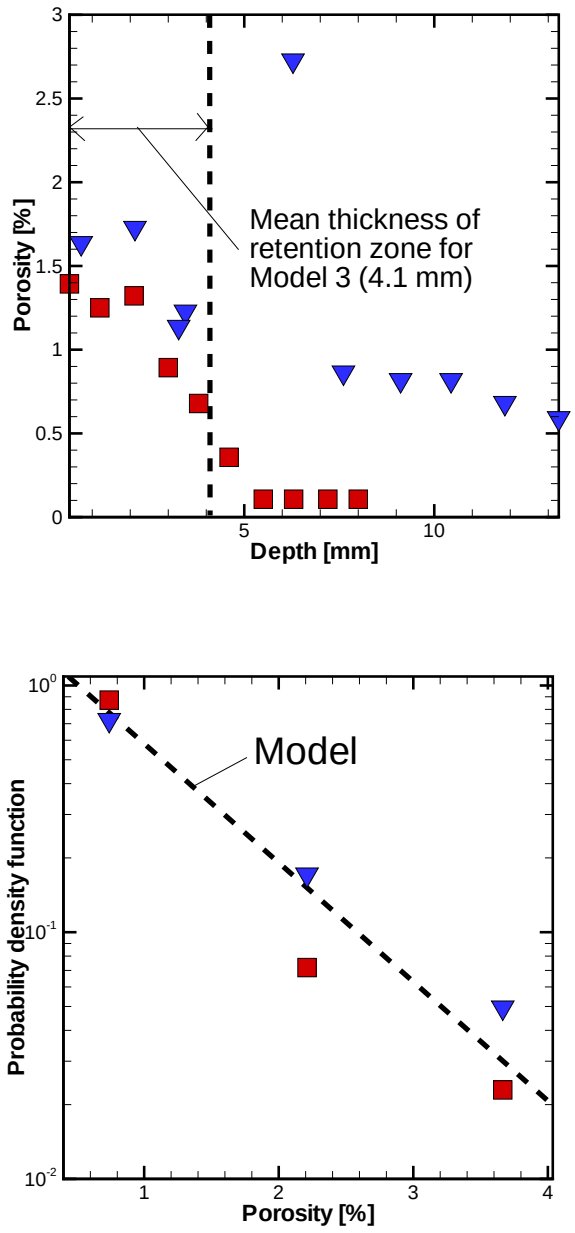

Figure 3.3: *Comparison of the mean thickness of the retention zone of 4.1 mm for Model 3 with two depth-dependent porosity data sets (a), and of the probability density function Eq.*(3.8) *for Model 3 (b), with two data sets of porosity distribution for a 25 cm^2 sample; data sets (denoted with different symbols) are from (Byegård et al., 2001).*

3.2 Injection conditions

We assume a general form of the injection as a pulse followed by an exponentially decaying tail:

$$\phi(t) = (1-\mu)\,\delta(t) + \frac{\mu}{d_0}\,\mathrm{e}^{-t/d_0} \qquad ; \qquad \widehat{\phi}(s) = (1-\mu) + \frac{\mu}{d_0}\,\frac{1}{s+1/d_0} \tag{3.10}$$

The two controlling parameters are the fraction μ which quantifies how much of the injected tracer mass is in the pulse and how much in the tail, and decay time d_0 [T] which quantifies the duration (or extent) of the tailing in the injection. For $\mu = 0$ we have a pure (ideal) pulse, whereas for $\mu = 1$, all injected mass is in the tail. For increasing d_0, a thinner tail extends over longer and longer times; for $d_0 \to 0$ we also recover a pulse.

In our following calculations, we shall assume $d_0 = 0.05$ years (440 h). Since $\ln 2\, d_0 = 0.035$ years (300 h) is the half-life of the injection tail (i.e., the time when half of the tracer mass contained in the tail has been released), we see that for $d_0 = 0.05$ y, the injection effectively terminates after ~ 1000 h. This is in the range that was applicable for the TRUE-1 experiments, at least for more sorbing tracers. Note that in the TRUE-1 tests, for instance, the injection tailing was initially not exponential, as a peak was visible after the pulse part of the injection terminates (Winberg et al., 2000). Although this peak is not captured by our current model, the measured asymptotic form of the injection tailing is reasonably approximated by exponential decay, Eq.(3.10).

3.3 Advective travel times

To apply Eq.(2.13), we require $f(\tau)$. Here we shall assume a Fickian (advection-dispersion) form of $f(\tau)$ as

$$f(\tau) = \frac{c\,\mathrm{e}^{c\sqrt{a}}}{2\sqrt{\pi\tau^3}}\,\exp\left(-a\,\tau - \frac{c^2}{4\,\tau}\right) \tag{3.11}$$

where

$$a \equiv \frac{\tau_m}{2\sigma_\tau^2} \qquad ; \qquad c \equiv \frac{\tau_m^{3/2}\sqrt{2}}{\sigma_\tau} \tag{3.12}$$

τ_m is the mean water residence time for a given flow path (i.e., averaged over all trajectories of a flow path), and σ_τ^2 is the variance. The Laplace transform of $f(\tau)$ Eq.(3.11) is

$$\widehat{f}(s) = \exp\left(c\,\sqrt{a} - c\sqrt{a+s}\right) \tag{3.13}$$

We shall assume in this analysis the coefficient of variation $CV(\tau) \equiv \sigma_\tau/\langle\tau\rangle = 0.5$ to be given (fixed), a value corresponding approximately to the estimated value of the TRUE-1 tests. Two values of the mean water residence time τ_m are to be considered in the computations, 10 h and 100 h; the former corresponds to a longer flow path and/or higher pumping rate, whereas the latter corresponds to a longer flow path and/or lower pumping rate.

Table 3.1: Summary of data for HTO, Ba and Cs used in the calculations.

TRACER	D_e $\times 10^{-6}$ [m^2/yr]	K_d [m^3/kg]
Tritium	1	–
Barium	1.3	0.001
Cesium	1.3	0.05

3.4 Tracer selection

We shall consider three tracers: tritium (HTO), barium (Ba) and cesium (Cs). The retention parameters D_w and K_d are tracer-dependent and are specified in Table 3.1. The values D_w are given in Byegård et al. (1998), while K_d are close to the calibrated values for TRUE-1 (Cvetkovic et al., 2000).

Chapter 4

Computations

For the computations, we shall use a discretized form of E Eq.(3.4); the full expression for E reads

$$E(s) = \Delta P \sum_{i}^{N} \sqrt{\theta_i^{2.5}\, D_w\, R_i}\ \left\{ \frac{\exp\left[2\,\zeta_i \sqrt{s\, R_i / D_w \sqrt{\theta_i}}\right] - 1}{\exp\left[2\,\zeta_i \sqrt{s\, R_i / D_w \sqrt{\theta_i}}\right] + 1} \right\} \tag{4.1}$$

where $\zeta_i \equiv \zeta(P_i)$, $\theta_i \equiv \theta(P_i)$, $R_i \equiv R(P_i)$, and $\zeta(P)$ and $\theta(P)$ are given in Eq.(3.5). We shall consider 50 segments (steps), i.e., $N = 50$, which implies that $\Delta P = 1/50 = 2\%$ is the probability significance margin.

Inserting Eq.(4.1) into Eq.(2.26) and then into Eq.(2.25), we have the final Laplace transform expression for h which needs to be inverted

$$\frac{\widehat{J}(s)}{m} = (1-\mu)\, \exp\left\{ \frac{\tau_m^2}{\sigma_\tau^2} \left[1 - \sqrt{1 + \frac{2\sigma_\tau^2}{\tau_m} \left(s + k\,\sqrt{s}\, E(s) \right)} \right] \right\} + \tag{4.2}$$

$$\frac{\mu}{d_0}\, \frac{1}{s + 1/d_0}\, \exp\left\{ \frac{\tau_m^2}{\sigma_\tau^2} \left[1 - \sqrt{1 + \frac{2\sigma_\tau^2}{\tau_m} \left(s + k\,\sqrt{s}\, E(s) \right)} \right] \right\}$$

where for a pulse we set $\mu = 0$.

If the parameters are constant, we use Eq.(4.2) with

$$E(s) = \sqrt{\theta^{2.5}\, D_w\, R}\ \frac{\exp\left[2\,\zeta \sqrt{s\, R / D_w \sqrt{\theta}}\right] - 1}{\exp\left[2\,\zeta \sqrt{s\, R / D_w \sqrt{\theta}}\right] + 1} \tag{4.3}$$

where it is understood that all parameters represent effective (uniform) values.

For the case of unlimited diffusion, we have

$$E = \langle \kappa \rangle \tag{4.4}$$

which is constant with respect to s.

Inverting $\widehat{J}$ Eq.(4.2), we get the normalized tracer discharge $J(t)/m$ which will be shown in the figures. For Laplace inversion, we use a code originally developed by J. Barker (British Geological Survey) and subsequently extended and used in Shapiro (2001) .

Chapter 5

Results

5.1 Tritium

Model 1

Breakthrough curves for the non-sorbing tracer Tritium are shown in Figures 5.1- 5.3. The curves in Figure 5.1 are based on Model 1 of retention heterogeneity (Figure 3.1), i.e., for a relatively thick retention zone (mean equal to 7.9 mm, Figures 3.1 and 3.2), and a relatively low porosity (mean equal to 1.2%, Figures 3.1 and 3.2). For pulse injection, we see that the tails of the BTCs diverge between the unlimited and limited diffusion models already after $\sim$90 h for mean water residence time of 10 h (Figure 5.1), and after $\sim$350 h for a longer flow path (or lower pumping rate) with mean water residence time of 100 h (Figure 5.1).

For finite injection where a pulse carrying 20% of the mass is followed by a relatively long tail carrying 80% of the tracer mass, the divergence of the tails in the BTCs between the limited and unlimited retention models occurs significantly later, after $\sim$2600 h. In fact, the divergence point in time of $\sim$2600 h is almost identical for the shorter and longer mean water residence times (10 h and 100 h, Figure 5.1). The reason for this is that for finite injection (Figures 5.1 with $\mu = 0.8$), the tail in the BTCs is maintained, not by diffusion in the rim zone, but by the injection characteristics. Thus the time when the tail attenuates asymptotically is independent of mean water residence time and depends only on injection conditions which are identical in both cases.

The curves in Figure 5.1 indicate that explicitly accounting for variability in retention parameters has no effect for Model 1 (blue and black solid lines overlap), and that the effective parameters are sufficient for accurately quantifying transport.

Model 2

Results for Tritium assuming Model 2 for the retention zone heterogeneity are given in Figure 5.2. Because Model 2 implies a relatively small retention zone with a comparatively high porosity (Figures 3.1 and 3.2), the divergence in the tail between the limited and unlimited diffusion models begins earlier than for Model 1. In particular, for pulse in-

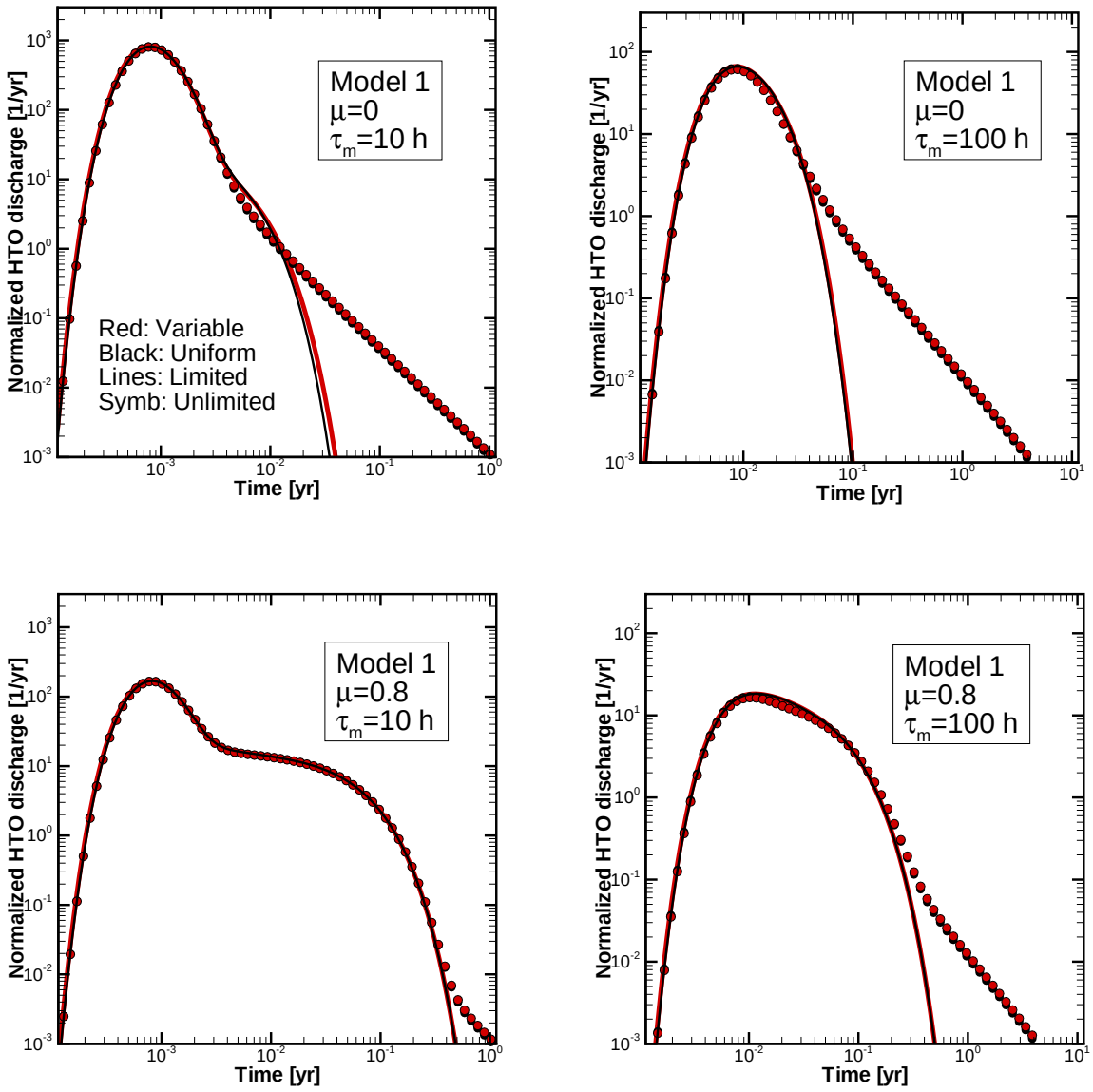

Figure 5.1: *Breakthrough curves for HTO assuming variability Model 1, for different mean water residence time τ_m, and injection conditions as quantified by the fraction μ in Eq.*(3.10).

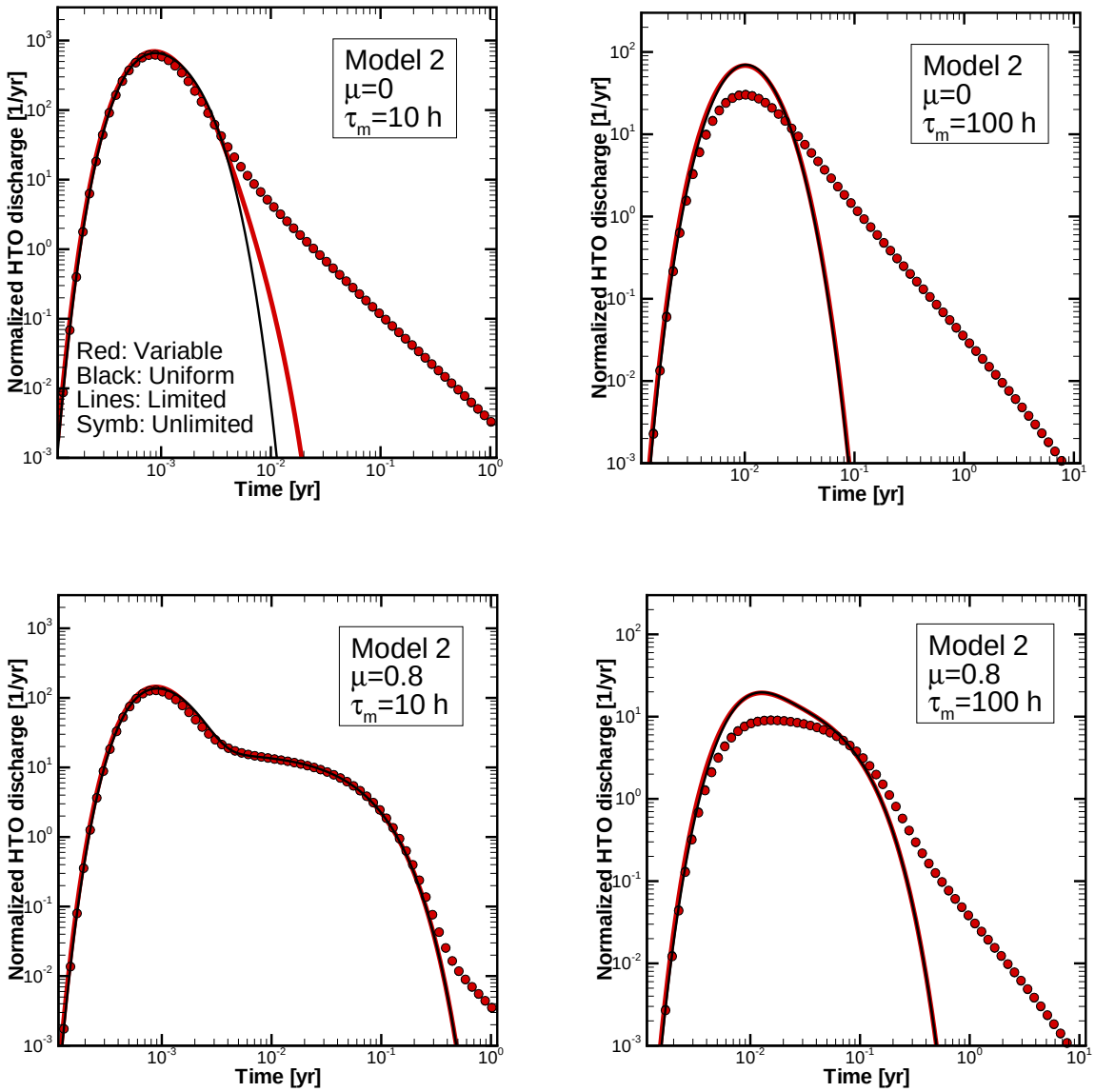

Figure 5.2: *Breakthrough curves for HTO assuming variability Model 2, for different mean water residence time τ_m, and injection conditions as quantified by the fraction μ in Eq.*(3.10).

jection and $\tau_m = 10$ h, the observable divergence occurs around 45 h (Figure 5.2), whereas for $\tau_m = 100$ h, it occurs after $\sim$260 h. For finite injection, the divergence point is again independent of τ_m, and is around 2600 h (Figures 5.2 with $\mu = 0.8$).

For Model 2, the variability in θ and ζ has some effect only for a pulse and τ_m=10 h, where using effective (uniform) parameters somewhat underestimates retention (difference between blue and black solid curves).

Model 3

Model 3 assumes ζ and θ are positively correlated along the flow path, with parameters that are consistent with available data (Figure 3.3). In this case, BTCs of HTO resemble those for Model 1, however, the "bump" in the tail appears somewhat earlier since Model 3 implies a smaller retention zone (compare BTCs of Figures 5.3 and 5.1). The divergence between the unlimited and limited diffusion tails in the BTCs starts for pulse injection already after 45 h for $\tau_m = 10$ h (Figure 5.3), and after 260 h for $\tau_m = 100$ h. If tracer injection is finite, then the divergence occurs after approximately 3500 h, irrespective of τ_m.

5.2 Barium

Model 1

Breakthrough curves for the moderately sorbing tracer Barium are shown in Figures 5.4-5.6. The curves in Figure 5.4 are based on Model 1 of retention heterogeneity (Figure 3.1), i.e., for a relatively large retention zone (mean 7.9 mm, Figure 3.2), and a relatively low porosity (mean 1.2%, Figure 3.2). The tails of the BTCs for the unlimited and limited diffusion models begin to diverge after 1 year for both $\tau_m = 10$ h and $\tau_m = 100$ h, and both the pulse and finite injection (Figure 5.4). After approximately 1 year, the characteristic "bump" appears (Figures 5.4 for $\tau_m = 100$ h), following which the tail of the BTC attenuates asymptotically, loosing its power-law (-3/2) dependence. In this case, the variability has no direct effect up to 1 year (blue and black curves are identical).

Model 2

Results for Barium assuming Model 2 for the retention zone heterogeneity are given in Figure 5.5. The divergence in the tail between the limited and unlimited diffusion models begins earlier than for Model 1, because the retention zone is smaller. The characteristic "bump" (raise) in the tail begins in the interval 450-550 h for a pulse with $\tau_m = 10$ h (Figure 5.5), and in the interval 550-900 h for a longer flow path (or lower injection rate) with $\tau_m = 100$ h. For finite injection, the observable evidence of diffusion limitations (change in the tail slope) appear later, in the interval 2600-4400 h for $\tau_m = 10$ h, and 850-1700 h, for $\tau_m = 100$ h (Figure 5.5).

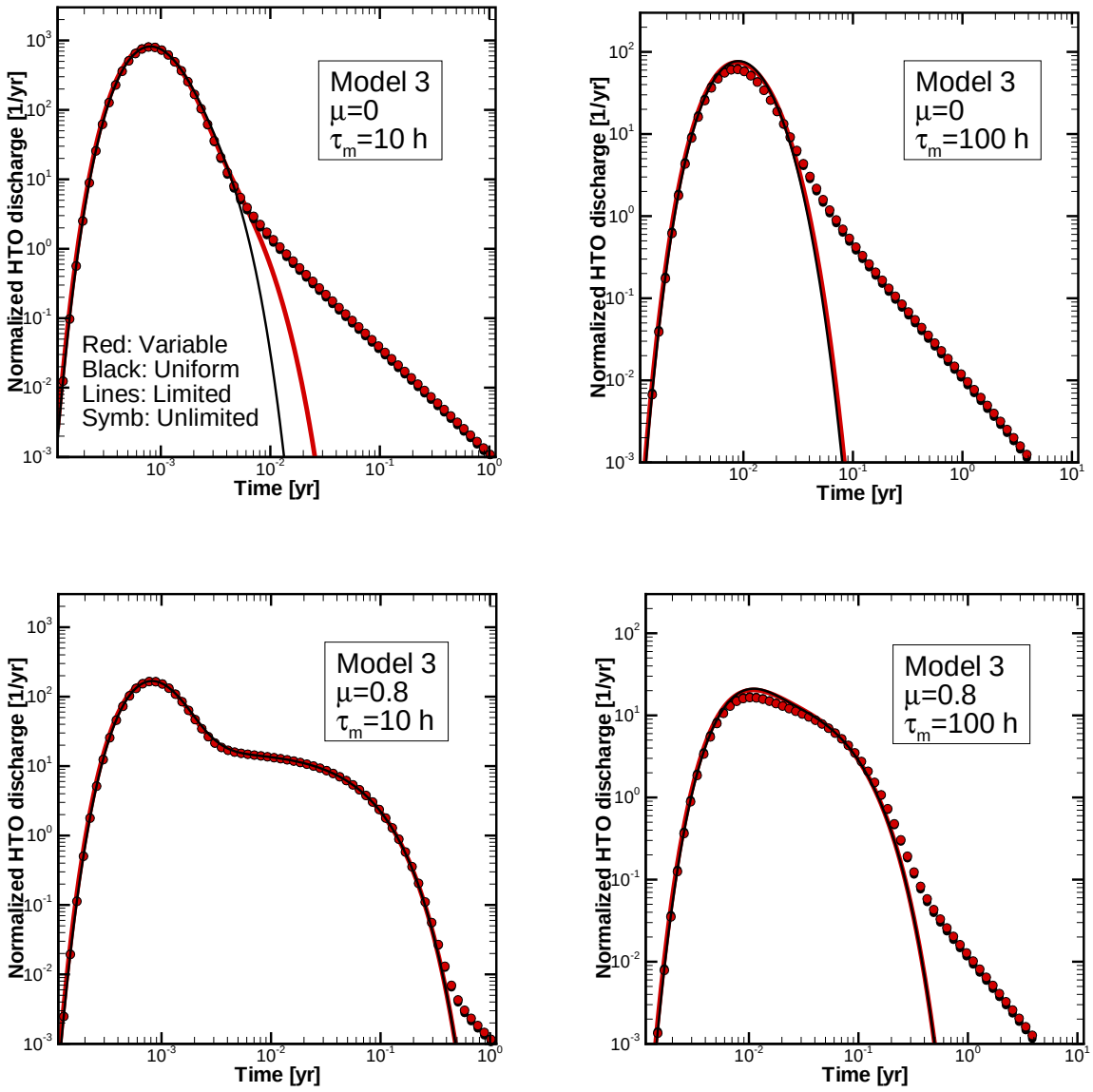

Figure 5.3: *Breakthrough curves for HTO assuming variability Model 3, for different mean water residence time τ_m, and injection conditions as quantified by the fraction μ in Eq.*(3.10).

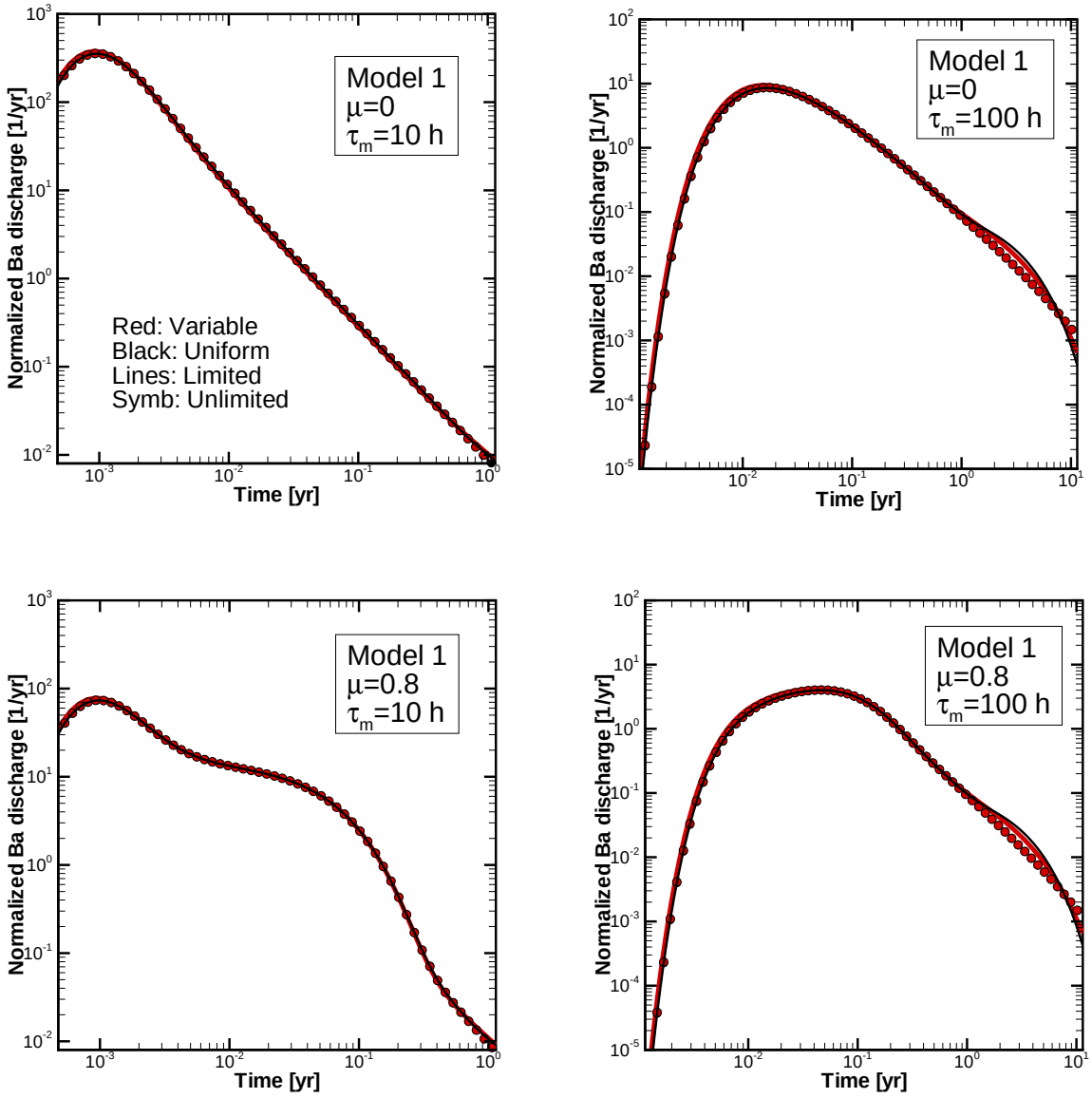

Figure 5.4: *Breakthrough curves for Ba assuming variability Model 1, for different mean water residence time τ_m, and injection conditions as quantified by the fraction μ in Eq.*(3.10).

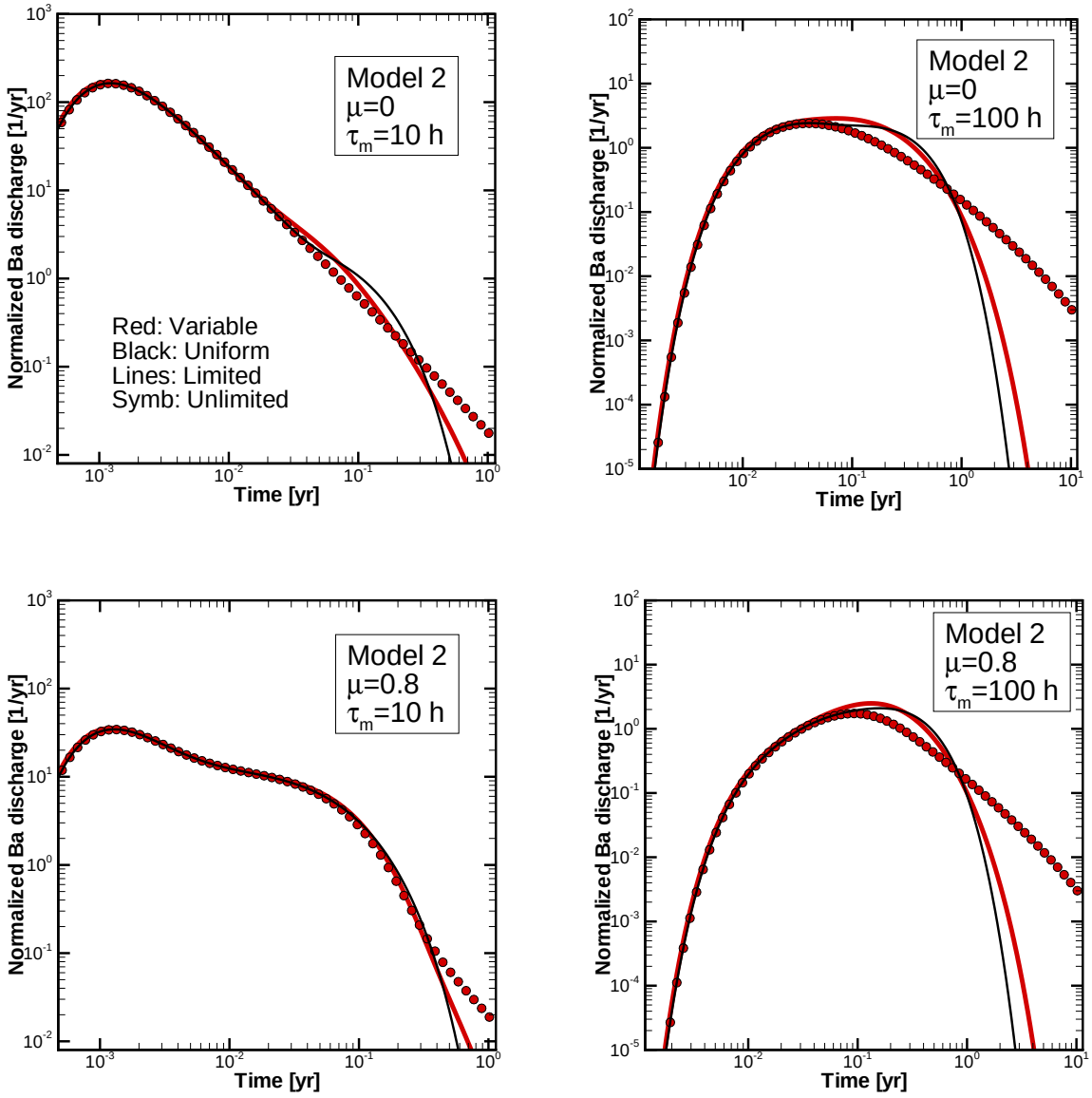

Figure 5.5: *Breakthrough curves for Ba assuming variability Model 2, for different mean water residence time τ_m, and injection conditions as quantified by the fraction μ in Eq.*(3.10).

Variability in θ and ζ along the flow path has some impact where the variable case predicts somewhat stronger retention visible in the tail part of the BTCs (difference between blue and black solid lines in Figure 5.4). However, this effect is still relatively small and would be difficult to discriminate.

Model 3

If ζ and θ are positively correlated along the flow path, with parameters that are consistent with available data (Model 3, Figures 3.1 and 3.3), then the BTCs (Figure 5.6) resemble those for Model 1 (Figure 5.4), but the "bump" in the tail appears somewhat earlier than for Model 1 (comparing Figures 5.4 and 5.6). For a pulse, the "bump" of limited diffusion appears around 2600 h for $\tau_m = 10$ h (Figure 9a) and similarly for $\tau_m = 100$ h (Figure 5.6). In the case of finite injection, evidence of diffusion limitations appear at a comparable time, around 2600 h for $\tau_m = 10$ h (Figure 5.6), and similarly for $\tau_m = 100$ h. The mean θ and ζ provide a accurate effective values for the considered time range (there is no distinction between blue and black solid lines).

5.3 Cesium

Model 1

Breakthrough curves for the strongly sorbing tracer Cesium are shown in Figures 5.7- 5.9. Model 1 assumes a relatively large retention zone (mean of 7.9 mm), and a relatively low porosity (mean 1.2%), hence the differentiation in the tail of the BTCs between the limited and unlimited diffusion model does not appear for a long time (Figure 5.7). The "bump" starts appearing after say 20-30 years, whereas the actual drop (or divergence) in the tails occurs approximately in the interval 100-200 years, irrespective of τ_m and the injection conditions (Figure 5.7).

Model 2

Model 2 implies a relatively small retention zone (mean 3.1 mm); consequently, the effect of diffusion limitations appears earliest and is most pronounced (Figure 5.8). For relatively short water residence times ($\tau_m = 10$) h, the tails diverge after approximately 10 years (Figures 5.8), whereas for longer water residence times $\tau_m = 100$ h, the divergence is apparent already after 1 year (Figure 5.8). However, the early divergence in the case with $\tau_m = 100$ h in Figure 5.8 is in the peak part of the BTC. Prior to the peak (which occurs after approximately 10 years), one cannot assess the slope of the tailing, and hence cannot distinguish between a limited and unlimited diffusion model. Variability in θ and ζ has some impact in the tail part of the BTCs, but only for relatively short water residence time $\tau_m = 10$ h (Figure 5.8 for τ_m =10 h, compare blue and black solid curves).

Model 3

If ζ and θ are positively correlated along the flow path, with parameters that are consistent with available data (Model 3), then the BTCs (Figure 5.9) resemble those for Model 1 (Figure 5.7), but the "bump" in the tail appears earlier than for Model 1 (compare Figures 5.7 and 5.9). The injection condition has no effect on BTCs in this case, only the mean water residence time. For $\tau_m = 10$ h, the "bump" that signifies limited diffusion effects appears

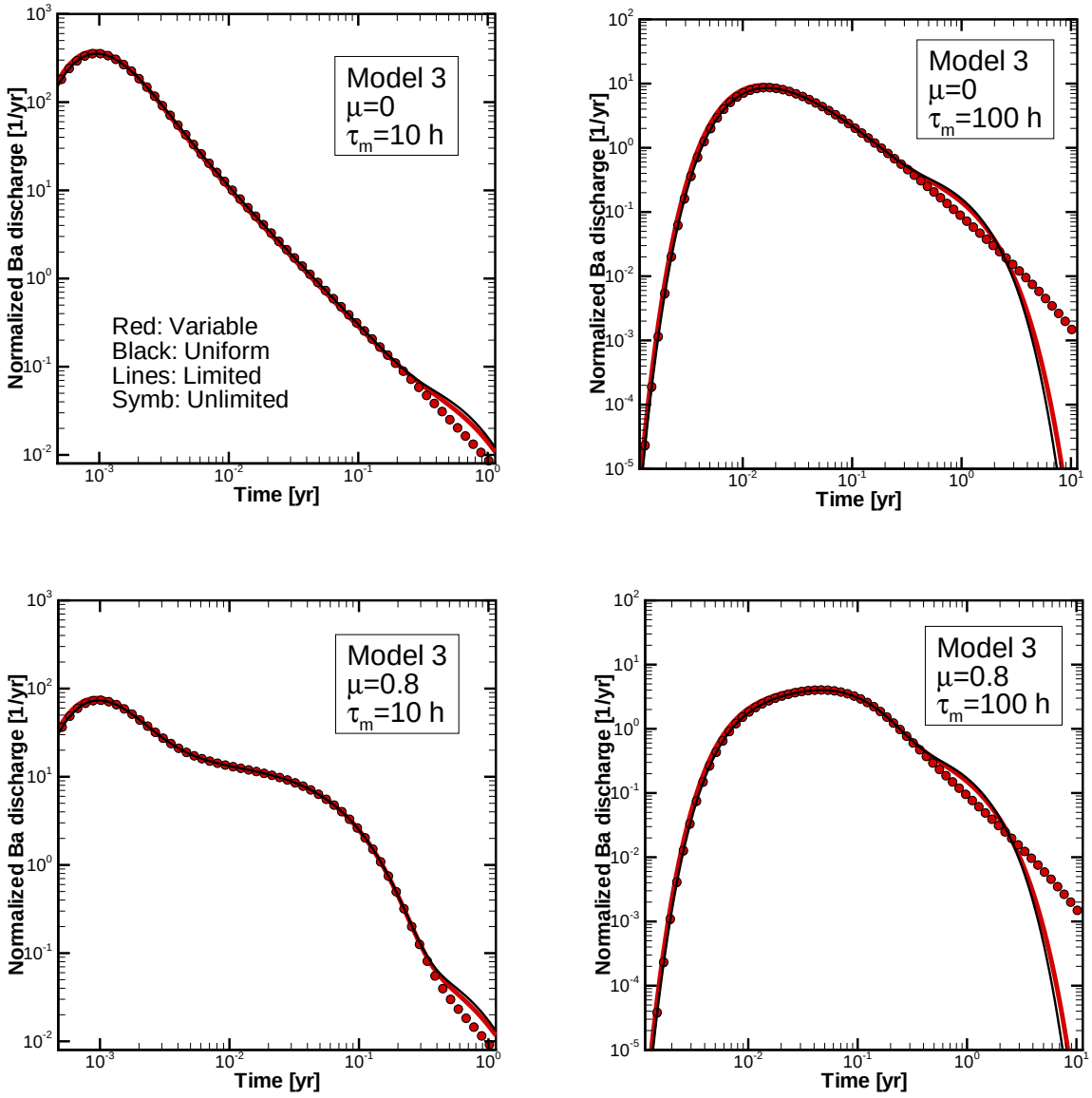

Figure 5.6: *Breakthrough curves for Ba assuming variability Model 3, for different mean water residence time τ_m, and injection conditions as quantified by the fraction μ in Eq.*(3.10).

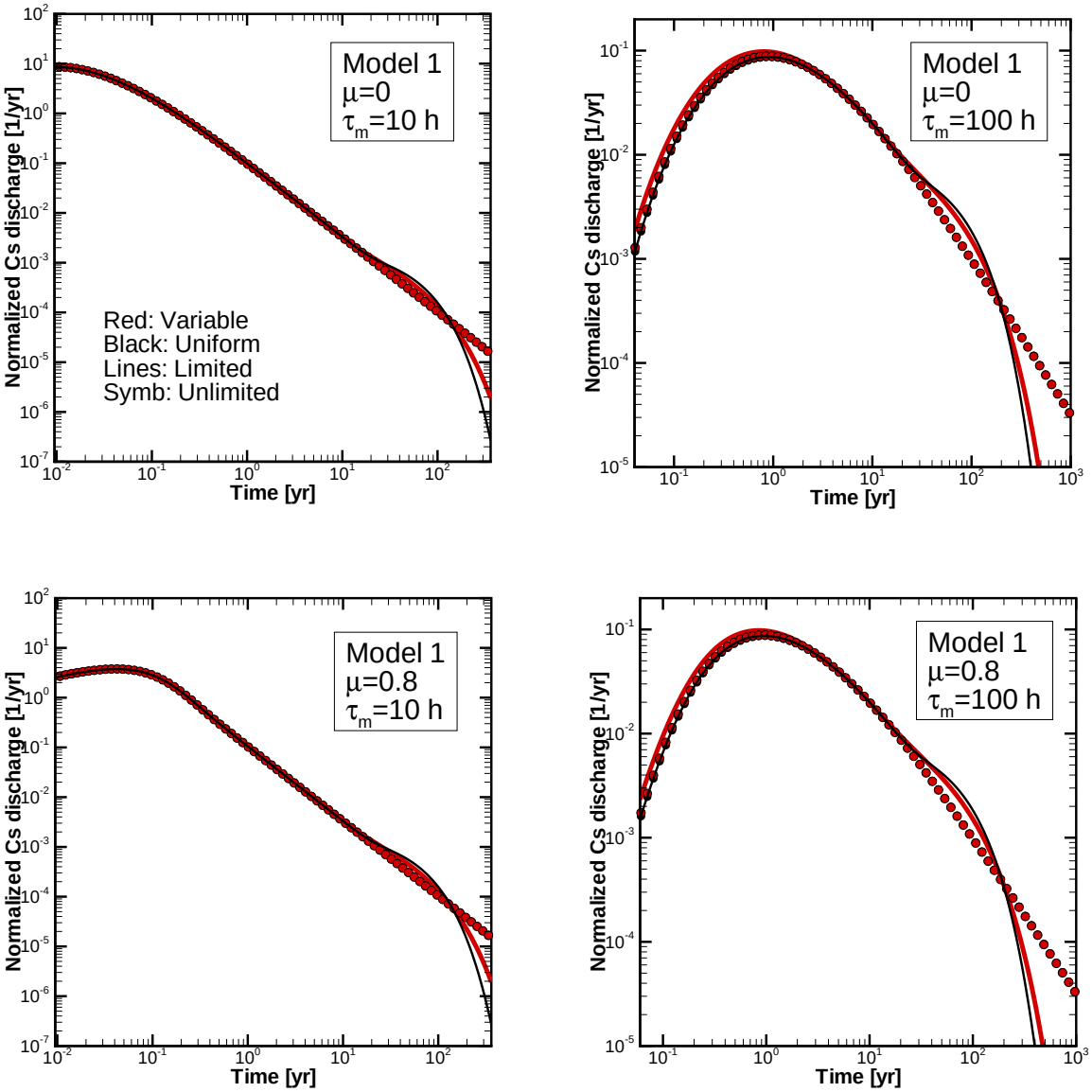

Figure 5.7: *Breakthrough curves for Cs assuming variability Model 1, for different mean water residence time τ_m, and injection conditions as quantified by the fraction μ in Eq.*(3.10).

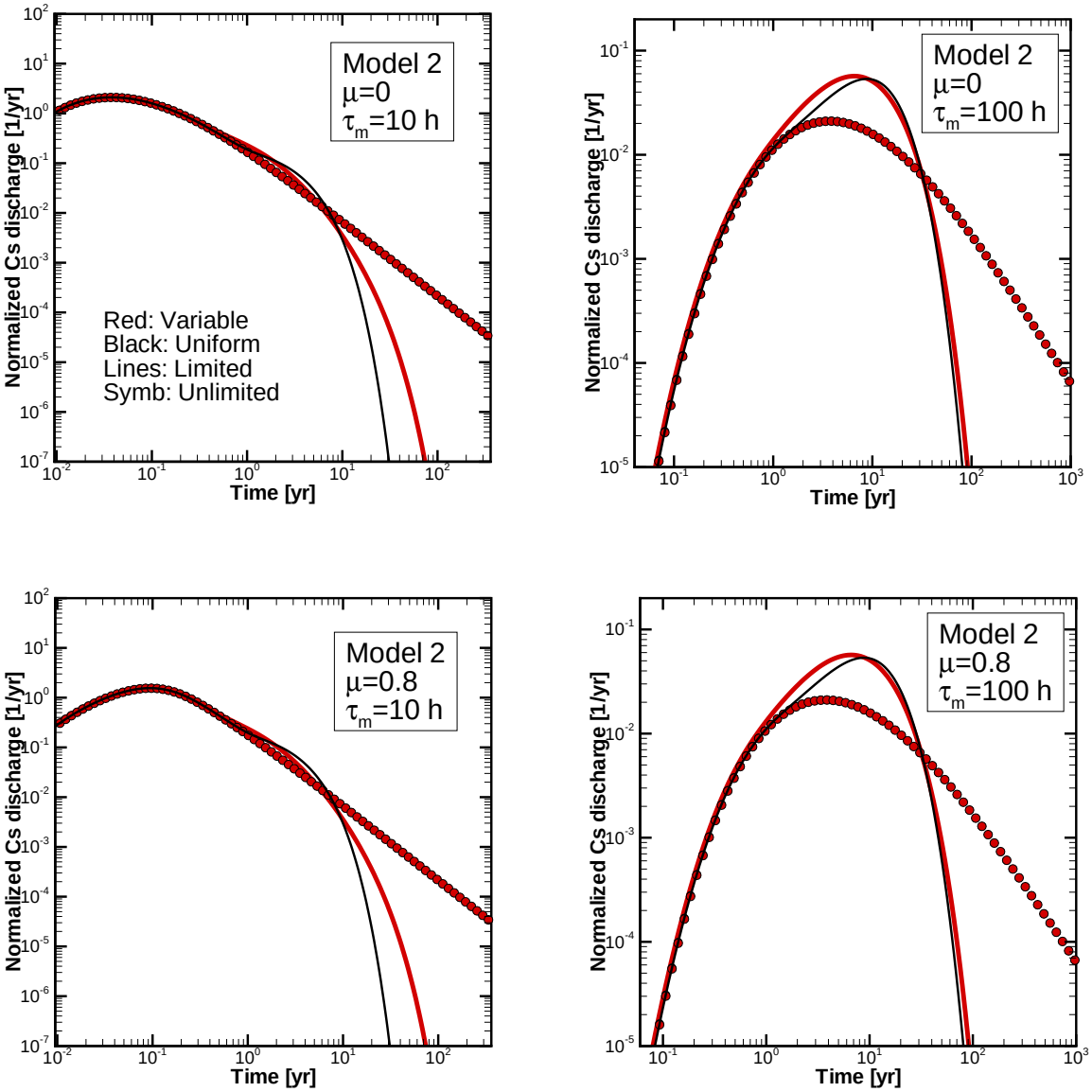

Figure 5.8: *Breakthrough curves for Cs assuming variability Model 2, for different mean water residence time τ_m, and injection conditions as quantified by the fraction μ in Eq.*(3.10).

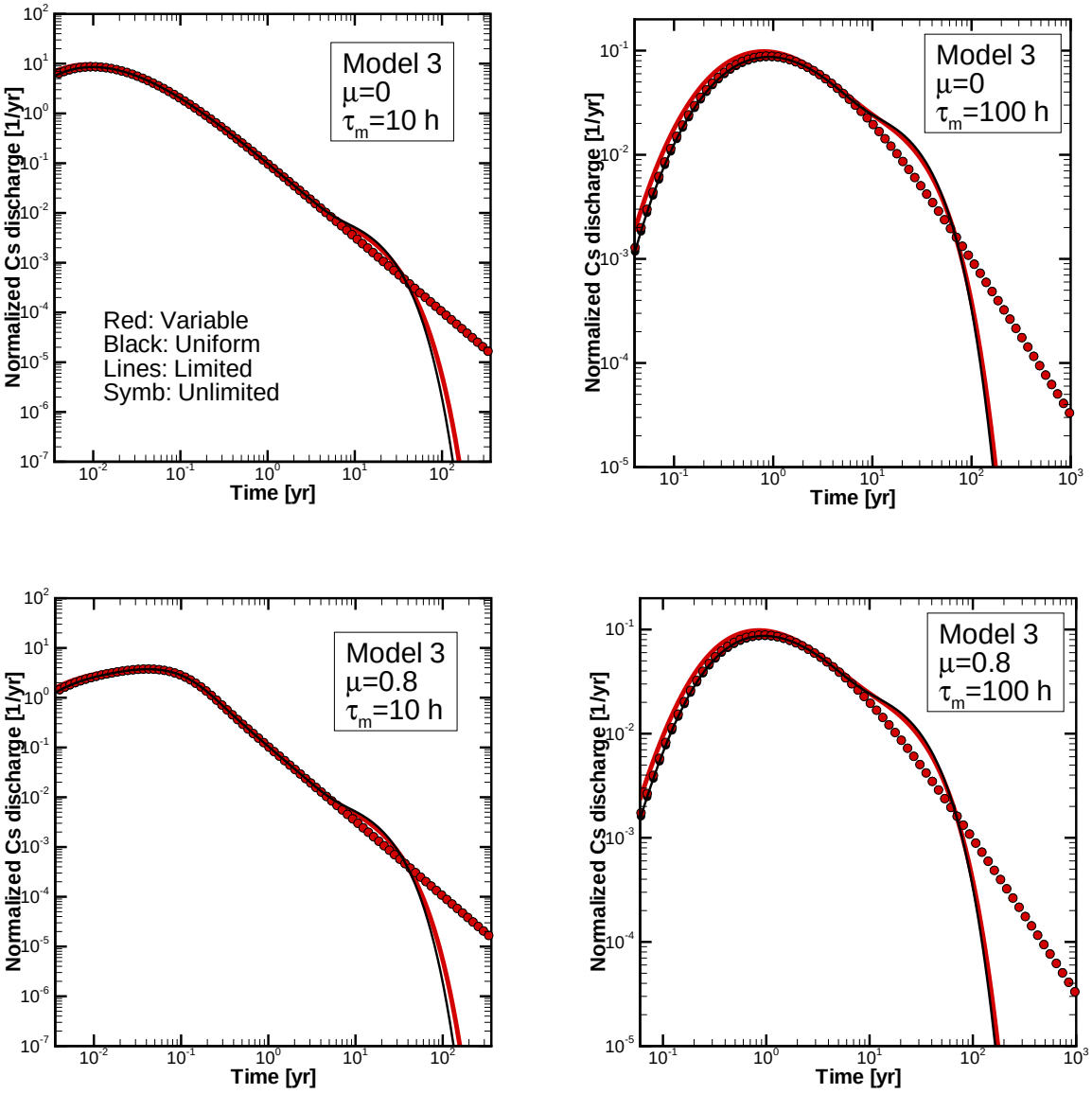

Figure 5.9: *Breakthrough curves for Cs assuming variability Model 3, for different mean water residence time τ_m, and injection conditions as quantified by the fraction μ in Eq.*(3.10).

in the interval 7-10 h for $\tau_m = 10$ h, similarly for $\tau_m = 100$ h (Figure 5.9). The mean θ and ζ provide accurate effective values for the considered time range (there is no distinction between blue and black solid lines).

Chapter 6

Summary and conclusions

We have presented a semi-analytical methodology for modelling tracer transport through rock fractures which accounts for the effect of diffusion limitations and rim zone heterogeneity on breakthrough curves. Using this methodology, we carried out a sensitivity analysis of potential effects for conditions comparable to the ones in TRUE-1 and TRUE Block Scale tracer tests, and identified the parameter ranges for which effects could be observable. The results of the sensitivity analysis are summarized in Tables 6.1-6.2.

Based on the obtained results we can draw the following conclusions.

- It is possible to analyze the combined effect of diffusion limitations and retention heterogeneity in a relatively simple and transparent manner, using the proposed methodology.
- The impact of diffusion limitations is exhibited as a rise (or "bump") in the BTC tail, followed by a relatively steep drop relative to the -3/2 (unlimited diffusion) slope. As an indicator of diffusion limitations, the "bump" is more apparent for tracers with increasing sorptivity; however, in practice the "bump" will be difficult to observe.

Table 6.1: Summary of results for Model 3 addressing the "observability" of the diffusion limitation effects. We consider "observable" a sufficient divergence in the tails (roughly defined as a factor of 2-3 on the log-log scale to account for possible fluctuations in the measurements) occuring up to approximately 1 year; tests longer than 1 year are therefore not considered practically feasible. Symbol "x" denotes an observable divergence, "-" possible but difficult, and "0" presumably not observable.

Tracer	$\tau_m = 10$ h Pulse inj.	$\tau_m = 10$ h Finite inj.	$\tau_m = 100$ h Pulse inj.	$\tau_m = 100$ h Finite inj.
HTO	x	-	x	-
Ba	0	0	0	0
Cs	0	0	0	0

Table 6.2: Summary of results for Model 3 as estimates of times when an observation of divergence in the tailing of the breakthrough could be made. Note that for Cs the observable divergence is not in the tail but before the peak.

Tracer	$\tau_m = 10$ h Pulse inj. [yr]	$\tau_m = 10$ h Finite inj. [yr]	$\tau_m = 100$ h Pulse inj. [yr]	$\tau_m = 100$ h Finite inj. [yr]
HTO	0.008	0.7	0.08	0.6
Ba	5	5	7	6
Cs	10	15	3	3

A more apparent indicator is the steep drop in the tail, i.e., the divergence of tails which occurs (sometimes significantly) later, following the rise.

- Finite injection (or tailing in the injection) will generally "mask" the impact of diffusion limitations, by making it much less apparent (or apparent much later), in particular for non-sorbing and weakly sorbing tracers. For HTO, for instance, effect of diffusion limitations would be apparent after 50 h if an ideal pulse was injected, and after almost one year if finite injection is applied.

- A rim zone up to 10 mm thick (4.1 mm in the mean) appears sufficient for observations of diffusion limitations to be virtually impossible for Cs, relatively difficult for Ba, and possible for HTO, even if there is tailing in the injection (as in TRUE-1) and the mean water residence time is in the range 10-100 h.

- Spatial variability in the rim zone thickness and porosity (diffusivity) has comparatively little impact on the BTCs, relative to the case where effective parameters are used (here defined as arithmetic mean).

- It is possible that the BTCs for HTO and weakly sorbing tracers measured in TRUE-1 and TRUE BS tracer tests, show some indications of diffusion limitations; however, further analysis of the measured BTCs, in the light of the present results, is required for a possible estimates of the rim zone thickness.

The presented methodology can be used in different ways. First, it can be applied in order to assess the possible impact of diffusion limitations on the expected breakthrough curves of the forthcoming tests TRUE BS2A in structure #19. With the water residence time specified, and the range of tracers specified, one could establish the potential effects of diffusion limitations and rim zone heterogeneity based on the available *in-situ* retention data. Second, one could re-evaluate the breakthrough curves of already completed tests (TRUE-1 and TRUE Block Scale), in order to assess possible evidence of diffusion limitations and estimate an average extent of the rim zone; it would be interesting to compare such an indirect estimate with a direct estimate from intercept data. Finally, the proposed methodology can be applied, say within Task 6 transport calculations, to assess the possible impact of diffusion limitations on long-term radionuclide transport. In this context, an

interesting task would be to develop simple ways of incorporating diffusion limitations for long term transport calculations, using for instance equilibrium retention in the rim zone (Cvetkovic et al., 1999), coupled to unlimited diffusion in the unaltered rock.

The semi-analytical methodology presented can be improved and/or extended in several ways.

- The intercept data used for Model 3 was based on the statistical variability analysis of a few samples. There is more similar data available which could be analyzed in order to define a better (or more representative) model for the rim zone thickness and porosity variability.

- We assumed a particular statistical model for the variability of the rim zone thickness and the porosity consistent with a few intercept data sets (Model 3), where we neglected potential correlation between the aperture and rim zone properties. The analysis could be extended to consider other statistical/variability models consistent with a larger data set, which could also account for some degree of correlation between aperture and rim zone properties.

- We limited the retention to the rim zone to highlight the effect of its limitation. A natural extension would be to also take into account the retention in the unaltered rock matrix, i.e., to couple diffusion/sorption in the rim zone and unaltered rock. This can be done either approximately using the analytical results of Cvetkovic et al. (1999), or exactly by solving numerically the diffusion into the rock matrix.

- The Lagrangian (trajectory) approach presented here can also be implemented as *Monte Carlo simulations* where either single fracture flow (Cvetkovic et al., 2000; Cheng et al., 2003), or discrete fracture network flow (Cvetkovic et al., 2003), is considered. In both cases, one needs to introduce overlapping random fields based on retention intercept data, and sum (integrate) along trajectories as for instance given in Eq. (2.16) or Eq. (2.17). Correlation between aperture and the retention parameters could in this way be accounted for directly in the simulations.

Bibliography

Byegård, J., Johansson, H., Skålberg, M., and Tullborg, E.-L. (1998). The interaction of sorbing and non-sorbing tracers with different Äspö rock types: Sorption and diffusion experiments in the laboratory scale. Technical Report TR-98-18, SKB.

Byegård, J., Widestrand, H., Skålberg, M., Tullborg, E., and Siitari-Kauppi, M. (2001). First TRUE Stage: Complementary investigation of diffusivity, porosity and sorptivity of Feature A-site specific geologic material. International Cooperation Report ICR-01-04, Swedish Nuclear Fuel and Waste Management Co.(SKB).

Cheng, H., Cvetkovic, V., and Selroos, J. (2003). Hydraulic control of retention in heterogeneous rock fractures. *Water Resources Research*, 39(5):1130, doi:10.1029/2002WR001354.

Cvetkovic, V. and Cheng, H. (2002). Evaluation of tracer retention understanding experiments on the block scale at Äspö. International Progress Report IPR-02-33, Swedish Nuclear Fuel and Waste Management Co.(SKB).

Cvetkovic, V., Cheng, H., and Selroos, J. (2000). Evaluation of tracer retentionn understanding experiments (first stage) at Äspö. International Cooperation Report ICR-00-01, Swedish Nuclear Fuel and Waste Management Co.(SKB).

Cvetkovic, V., Dagan, G., and Cheng, H. (1998). Contaminant transport in aquifers with spatially variable hydraulic and sorption properties. *Proceedings of the Royal Society of London*, 454:2173–2207.

Cvetkovic, V. and Haggerty, R. (2002). Transport with exchange in disordered media. *Physical Review E*, 65:051308–1–9.

Cvetkovic, V., Painter, S., Outters, N., and Selroos, J. (2003). Stochastic simulation of radionuclide migration in discretely fractured rock near the äspö Hard Rock Laboratory. *Water Resources Research*. to appear.

Cvetkovic, V., Selroos, J. O., and Cheng, H. (1999). Transport of reactive tracers in rock fractures. *Journal of Fluid Mechanics*, 378:335–356.

Dagan, G. (1984). Solute transport in heterogeneous porous formations. *Journal of Fluid Mechanics*, 145:151–177.

Kelokaski, M., Oila, E., and Siitari-Kauppi, M. (2001). Investigation of porosity and microfracturing in granitic rock using the 14C-PMMA technique on samples from the TRUE Block Scale site at the Äspö Hard Rock Laboratory. International Progress Report IPR-01-27, Swedish Nuclear Fuel and Waste Management Co.(SKB).

Neretnieks, I. (1980). Diffusion in the rock matrix: An important factor in radionuclide retention. *Journal of Geophysical Research*, 85(B8):4379–4397.

Shapiro, A. (2001). Effective matrix diffusion in kilometer-scale transport in fractured crystalline rock. *Water Resources Research*, 37:507–522.

Winberg, A., Andersson, P., Hermanson, J., Byegård, J., Cvetkovic, V., and Birgersson, L. (2000). Final report on the first stage of the tracer retention understanding experiments. Technical Report TR-00-07, Swedish Nuclear Fuel and Waste Management Co.(SKB).